

Energy and Charged Particle Flow in 10.8 A GeV/c Au+Au Collisions

J. Barrette⁴, R. Bellwied⁸, S. Bennett⁸, P. Braun-Munzinger⁶, W. C. Chang⁶,
W. E. Cleland⁵, M. Clemen⁵, J. Cole³, T. M. Cormier⁸, G. David¹, J. Dee⁶, O. Dietzsch⁷,
M. Drigert³, J. R. Hall⁸, T. K. Hemmick⁶, N. Herrmann², B. Hong⁶, Y. Kwon⁶,
R. Lacasse⁴, A. Lukaszew⁸, Q. Li⁸, T. W. Ludlam¹, S. K. Mark⁴, R. Matheus⁸,
S. McCorkle¹, J. T. Murgatroyd⁸, E. O'Brien¹, S. Panitkin⁶, T. Piazza⁶, C. Pruneau⁸,
M. N. Rao⁶, M. Rosati⁴, N. C. daSilva⁷, S. Sedykh⁶, U. Sonnadara⁵, J. Stachel⁶,
E. M. Takagui⁷, S. Voloshin^{5*}, G. Wang⁴, J. P. Wessels⁶, C. L. Woody¹, N. Xu⁶,
Y. Zhang⁶, C. Zou⁶

(E877 Collaboration)

¹ *Brookhaven National Laboratory, Upton, NY 11973*

² *Gesellschaft für Schwerionenforschung, Darmstadt, Germany*

³ *Idaho National Engineering Laboratory, Idaho Falls, ID 83402*

⁴ *McGill University, Montreal, Canada*

⁵ *University of Pittsburgh, Pittsburgh, PA 15260*

⁶ *SUNY, Stony Brook, NY 11794*

⁷ *University of São Paulo, Brazil*

⁸ *Wayne State University, Detroit, MI 48202*

(November 26, 2024)

Abstract

Experimental results and a detailed analysis are presented of the transverse energy and charged particle azimuthal distributions measured by the E877

*On leave from Moscow Engineering Physics Institute, Moscow, 115409, Russia

collaboration for different centralities of Au+Au collisions at a beam momentum of $10.8 A \text{ GeV}/c$. The anisotropy of these distributions is studied with respect to the reaction plane reconstructed on an event-by-event basis using the transverse energy distribution measured by calorimeters. Results are corrected for the reaction plane resolution. For semicentral events we observe directed flow signals of up to ten percent. We observe a stronger anisotropy for slow charged particles. For both the charged particle and transverse energy distributions we observe a small but non zero elliptic anisotropy with the major axis pointing into the reaction plane. Combining the information on transverse energy and charged particle flow we obtain information on the flow of nucleons and pions. The data are compared to event generators and the need to introduce a mean field or nucleon-nucleon potential is discussed.

I. INTRODUCTION

Collisions between two gold nuclei of about $11 \text{ A} \cdot \text{GeV}/c$ momentum at the AGS have been characterized rather completely in terms of the global observables, transverse energy E_T [1] and charged particle multiplicity N_c [2]. The picture that emerged from these measurements is that the two gold nuclei stop each other to a very high degree. Through comparison to models that reproduce the experimental observables initial particle and energy densities have been inferred and maximum values around ten times normal nuclear matter density and $2 \text{ GeV}/\text{fm}^3$ have been found [3–5]. On the other hand, hadrons cease to interact strongly and freeze-out at a density significantly below nuclear matter density (for Si + Au collisions at the AGS see [6]). The interesting question arises to what degree the system loses its memory of the initial highly compressed phase during the subsequent expansion.

While particle yields are consistent with chemical equilibrium already for the lighter Si + Au system [6], particle spectra show that the equilibrium is only local and that overall the system expands longitudinally and transversely with an average velocity of one half and one third of the speed of light [6], respectively. Recently we found from analyzing the azimuthal asymmetry of the transverse energy distribution that the system even remembers the initial collisions geometry or the impact parameter: for all but the most peripheral and the most central collisions a dipole component also called ‘sideward flow’ is observed in the transverse energy azimuthal distribution forward and backward of mid-pseudorapidity [7]. The forward and backward flow effects are back-to-back or 180° relative to each other. The effect is largest in semicentral collisions. Integrating over pseudorapidities forward of $\eta = 1.85$, about 9% of the transverse energy is carried by this directed flow [7].

Following up on the initial discovery of this sideward flow at AGS energies our goal is to characterize the effect in more detail in order to eventually gain access to the equation of state of nuclear matter at the extreme densities reached initially in gold-gold collisions at $11 \text{ A} \cdot \text{GeV}/c$. In this paper, we present a complete characterization of the flow behavior in transverse energy and charged particle multiplicity with fine binning in pseudorapidity

and as a function of centrality of the collision. At the same time we are studying the triple differential cross section of the emission of identified particles such as protons and pions in the E877 forward spectrometer [8]. This will be the subject of a future publication. In the following Chapter we will briefly describe the experimental set-up and conditions, and introduce the analysis method in Chapter 3. The resulting anisotropies are presented in Chapter 4. In Chapter 5, we analyse the flow signal from one of the cascade codes (RQMD [9]) that describe the collisions in terms of individual hadron-hadron collisions and compare this prediction to the experimental data. In Chapter 6 we use the complementarity of the two measurements (in multiplicity N_c and in transverse energy E_T) to disentangle the contribution of pions and nucleons to the observed flow signals and to again compare to model predictions as well as to lower energy data.

II. EXPERIMENT

In the experiment presented here a 10.8 A· GeV/c Au beam of the Brookhaven AGS was impinging on Au targets of 540 and 980 mg/cm² areal density corresponding to 1.07 and 1.94 % of a Au + Au nuclear interaction length. The reaction products were detected in the E877 apparatus schematically depicted in Figure 1. The detectors used in the present analysis are shown enlarged in the insert. In the fall 1993, AGS heavy-ion run information from about 10⁷ Au + Au collisions was collected sampling the whole impact parameter range with parallel triggers requiring different levels of E_T or just the presence of a beam particle.

Every incident beam particle is characterized by the scintillator hodoscope (S1-S4), and the horizontal position and angle of incidence at the target are measured by a pair of silicon microstrip detectors (BVER1,2). The method used to correct for the beam displacement and direction is described in detail in [2]. The angular divergence of the beam is of the order of 1 mr and much smaller than the bin width in η and ϕ used in the present analysis. Interactions occurring upstream of the target are effectively rejected by requiring (i) that the pulseheight measured in a 100 μ m thick silicon detector just upstream of the target is

consistent with the energy loss of a Au ion, (ii) that a (beam) particle in BVER1,2 is not accompanied by other tracks, and (iii) that the correlation between E_T measured in different ranges of pseudorapidity η follows the systematics for interactions in the target (see below).

The event characterization is obtained using the transverse energy measured in the two calorimeters surrounding the target, the target calorimeter (TCal) and participant calorimeter (PCal). The TCal consists of NaI crystals of 5.3 radiation lengths depth. In the present analysis the pseudorapidity range $-0.5 \leq \eta \leq 0.8$ is used to measure transverse energy in 13×64 bins in η and azimuthal angle ϕ . For more details on the TCal and the analysis of TCal data see [1,10,11]. The E_T measurement at central and forward rapidity is obtained using the PCal, a lead/iron/scintillator sampling calorimeter described in [1,12]. The PCal has full azimuthal coverage with a granularity of $\Delta\phi = 20^\circ$. In pseudorapidity data are obtained for 17 bins covering $0.9 \leq \eta \leq 4.2$ (see Figure 2). The 4 depths sections of the calorimeter are not used separately in the present analysis. The orientation of the reaction plane is determined event-by-event using E_T from the TCal or one of several η regions of the PCal. The azimuthal distribution of E_T relative to the reaction plane is then determined over the full range of $-0.5 \leq \eta \leq 4.2$.

The distribution of charged particles N_c is measured in two identical silicon pad detectors of 300 μm thickness. The placement and segmentation of the silicon detectors is shown in Figure 3. Each detector is segmented into 512 pads with 8×64 bins in η and ϕ of typically 100 mr width. The azimuthal distribution of the charged particle emission relative to the reaction plane is measured in 12 bins for $0.8 \leq \eta \leq 2.65$. An analysis of the N_c distribution as a function of centrality in Au + Au collisions is published in [2]. Details of the analysis technique, e.g. how to deal with δ -rays, multiple hits, beam displacement, can be found there and were adopted for the present analysis as well. The present data are not corrected for γ conversion (carrying the flow information of π^0) which in the analysis presented below accounts for about 6 % of the hits in the silicon pad detectors.

III. FLOW ANALYSIS

The azimuthal anisotropy is analysed as a function of the centrality of the collision. Centrality is measured by E_T in the calorimeters. Figure 4a displays for both detectors the fraction of the geometric cross section $\sigma_{top}(E_T)/\sigma_{geo}$ obtained by integrating from a given value of E_T to the maximum E_T observed. Here the geometric cross section is defined as $\sigma_{geo} = \pi r_0^2(A^{1/3} + A^{1/3})^2 = 6.127$ b with the mass number $A = 197$ and $r_0 = 1.2$ fm. Both distributions are not unfolded for detector response. The shape of the distributions is very similar for the two detectors except that the fall-off for very central collisions is somewhat wider for the TCal because of the smaller η coverage and larger leakage fluctuations. Figure 4b shows the projection of the correlation between the two E_T measurements on either axis with error bars indicating the width (standard deviation) of the correlation. The correlation is close to linear over most of the range and only for collisions in the top 5 % range of centrality does one or the other centrality measure select different events. Also shown in the figure are the E_T bins used in the analysis. The most peripheral bins start at 5 and 50 GeV in TCal and PCal, respectively, i.e. only the top half of the geometric cross section is studied. The results presented later have been corrected for interactions not occurring in the target and the correction to the resulting anisotropies is noticeable only for the more peripheral collisions with PCal $E_T \leq 100$ GeV.

In our previous analysis of the azimuthal anisotropy of E_T production [7] we have subdivided the data into η bins and have performed, event-by-event, a Fourier analysis [13] of the azimuthal distribution in each η bin. This method has the advantage that it involves only one η interval at a time and that it does not require to determine a reaction plane angle. Hence it is not influenced by the resolution with which different detectors can measure the reaction plane angle. However, since the Fourier analysis is performed for every event, the size of the η bin has to be large enough to allow to distinguish a true anisotropy from a statistical fluctuation. In central Au + Au collisions the total multiplicity reaches indeed large values of 800 - 900 over the full solid angle. However, first results on the centrality de-

pendence of the anisotropy [7] found the effect to be maximal in semi-central collisions where the multiplicity is significantly lower. In practice, this was limiting our previous analysis to three η bins. Since we did indeed see a pronounced first (or dipole) moment with a strong back-to-back correlation of forward and backward η bins we choose a different strategy in the present analysis to now study the flow effects in small η bins.

From the data, the azimuthal angle $\Psi_n^{(i)}$ of the n -th moment of the transverse energy distribution in the η window i is obtained via

$$\tan \Psi_n^{(i)} = \frac{\sum_j (\pm) E_T^j \sin n\phi_j}{\sum_j (\pm) E_T^j \cos n\phi_j} = \frac{\sum_j (\pm) E_{Tx}^j}{\sum_j (\pm) E_{Ty}^j} \quad (1)$$

where the sum runs over the j cells with azimuthal angles ϕ_j of the detector in an η window i and the sign is positive (negative) for cells at η forward (backward) of mid-pseudorapidity. For $n=1$ this is the equivalent of the directivity method used in [14], except that we use E_T instead of p_t .

For every event, the angle $\Psi_1^{(i)}$ of the dipole component is found in the i -th of four pseudorapidity windows. The most backward window W1 covers the range $-0.5 \leq \eta \leq 0.7$, where the TCal has full azimuthal coverage. The windows W2, W3, and W4 label regions of the PCal covering approximately $0.8 \leq \eta < 1.4$, $2.0 \leq \eta < 2.7$, and $2.7 \leq \eta < 4.5$. Here the region around midrapidity is intentionally skipped since the dipole component is expected to cross zero in that region. We denote by Ψ_R the angle the reaction plane (defined by the impact parameter \vec{b} and the beam direction \hat{z}) makes with the laboratory x -axis (see Figure 1). The angles $\Psi_1^{(i)}$ are the experimental measure of Ψ_R . A remaining twofold ambiguity is solved by defining that in the forward hemisphere Ψ_1 points in the direction of \vec{b} , where \vec{b} points from target to projectile. This is consistent with the assumption that the projectile scatters away from the target (repulsive trajectory). The angle Ψ_1 is shifting by a phase of π at midrapidity. We have experimentally verified this back-to-back correlation [7]. Neglecting the phase information, Ψ_1 is generally called the reaction plane angle and we will stay with this terminology. Since there is only one reaction plane orientation for every

collision a comparison of the angles $\Psi_1^{(i)}$ measured in the four η windows allows to extract the resolution with which Ψ_R is measured in each window.

The azimuthal distribution with respect to the reaction plane angle of a global observable X is expanded in terms of its Fourier components

$$\frac{d^2 X}{d\eta d(\phi - \Psi_R)} = v_0 \left(1 + \sum_{n \geq 1} (2v_n \cos n(\phi - \Psi_R)) \right), \quad (2)$$

where $v_0 = \langle X \rangle_\eta / 2\pi$ and $\langle X \rangle_\eta$ is the average of the observable X in the pseudorapidity interval $d\eta$. Note that sine terms are missing because of the necessary reflection symmetry with respect to the reaction plane. This expansion is equivalent to a decomposition into multipole components in a plane (transverse to the beam direction).

A Fourier decomposition of the distribution X measured with respect to the reaction plane angle determined in the i -th window yields

$$\frac{d^2 X}{d\eta d(\phi - \Psi_1^{(i)})} = v_0 \left(1 + \sum_{n \geq 1} (2v'_n \cos n(\phi - \Psi_1^{(i)})) \right) \quad (3)$$

and for practical reasons we limit the analysis to $n=1,2$ (see below). The Fourier coefficients in this series are evaluated by fitting equation (3) to the data or from:

$$v'_n = \frac{\langle \sum_k X^k \cos n(\phi_k - \Psi_1^{(i)}) \rangle}{\langle \sum_k X^k \rangle}, \quad (4)$$

where the sum is taken over all cells of the detector belonging to a pseudorapidity bin under study, and the brackets refer to the event average evaluated for a given event class (centrality).

From the measured Fourier coefficients v'_n the true values v_n can be obtained (see also [13]) by unfolding for the finite resolution with which Ψ_R is measured, using

$$v_n = \frac{v'_n}{|\langle \cos n(\Psi_1^{(i)} - \Psi_R) \rangle|}. \quad (5)$$

Again the brackets indicate the event average evaluated for a given pseudorapidity window and a given event class (centrality). The measurement of $\Psi_1^{(i)}$ in three or more pseudorapidity

windows (four in our case) allows to evaluate the correction factors $\langle \cos n(\Psi_1^{(i)} - \Psi_R) \rangle$ directly from the data without further assumptions. We have, e.g. for $n=1$,

$$\cos(\Psi_1^{(i)} - \Psi_1^{(j)}) = \cos(\Psi_1^{(i)} - \Psi_R) \cos(\Psi_1^{(j)} - \Psi_R) + \sin(\Psi_1^{(i)} - \Psi_R) \sin(\Psi_1^{(j)} - \Psi_R). \quad (6)$$

Taking the event average, using the reflection symmetry of the ϕ distribution with respect to the reaction plane and assuming that the only correlation between pseudorapidity windows i and j is via the flow effect we obtain

$$\langle \cos(\Psi_1^{(i)} - \Psi_1^{(j)}) \rangle = \langle \cos(\Psi_1^{(i)} - \Psi_R) \rangle \langle \cos(\Psi_1^{(j)} - \Psi_R) \rangle. \quad (7)$$

Combining these equalities for the four pseudorapidity windows we can evaluate the effect of the finite reaction plane resolution in window i as a function of centrality. The results are shown in Figure 5. The resolution in a given η interval is determined by the finite granularity, the energy resolution and leakage fluctuation of the detector, and the magnitude of the anisotropy in this η interval. The symbols in the left diagram reflect the correction to be applied to the measured dipole component. The correction is smallest for semicentral collisions (PCal $E_T \approx 220$ GeV) where we found the flow effect to be largest [7]. Comparing the different pseudorapidity windows, the resolution is best for the most forward window W4 but W3 and W1 also give satisfactory results. In the window W2 the correction is rather sizeable as expected, more than a factor of two for all centralities, and we discard for the following analysis this window for purposes of reaction plane determination. The signs of the correction factors reflect the phase shift by π in the angles Ψ_1 at mid-pseudorapidity.

The effect of finite reaction plane resolution becomes more significant for higher multipole components as displayed on the right hand side of Figure 5 for the quadrupole component. There, only the two forward PCal windows yield manageable corrections of about a factor two for semicentral collisions and a factor four to six for central collisions. This shows the difficulty to extract any multipole components with $n \geq 3$ from the data by methods involving the determination of a reaction plane. Our previous method [7] of event-by-event Fourier decomposition does not have this limitation but is limited by the finite multiplicity in an event which depends *e.g.* on the beam energy and centrality of the collision.

One may ask to what extent the accuracy of the correction is affected by remaining detector imperfections such as, e.g., miscalibrated or missing calorimeter channels which may bias the distribution of $(\Psi_1^{(i)} - \Psi_1^{(j)})$. We have studied this question by generating a probability distribution in angle difference normalized to a probability distribution from 'mixed events' where the two angles are from different events. Using this probability distribution in the averaging procedure yields, for W4 for instance, the histogram presented in Fig. 5 as compared to the points. The differences are small, typically 5 % or less for all four pseudorapidity windows.

Analyzing the calorimeter data care has to be taken to assign the proper pseudorapidity value to each tower of the calorimeter. The spread of showers, the nonprojective geometry of a detector, and the variation in the E_T distribution over the solid angle covered by a detector cell will, in general, result in an effective mean pseudorapidity, which is different from the pseudorapidity of the center of the tower. As in [1] we have simulated the PCal performance using the GEANT [15] package combined with an event generator that reproduces the measured E_T distribution and with a fast shower deposition code PROPHET [16]. The pseudorapidity distributions of the particles which contribute to each PCal tower were calculated. The mean value of pseudorapidity weighted with the deposited energy was determined and used later in the analysis as the tower pseudorapidity. In Figure 6 we show how the assigned η values differ from the pseudorapidity of the cell geometrical center. We also show in this figure the spread of η values (standard deviation) of particles contributing to the energy deposit in a given tower. This gives an indication that structures in the azimuthal anisotropy of the E_T distribution cannot be resolved to better than about 0.5 units of pseudorapidity. Using different, realistic event generators and different centralities of the collision we checked that the assigned pseudorapidity values are not visibly model or centrality dependent. The differences in mean values for different event generators/centralities are much less than the widths shown in the figure, and for the midrapidity region were found to be less than 0.05.

IV. AZIMUTHAL DISTRIBUTIONS OF CHARGED PARTICLES AND TRANSVERSE ENERGY

A. Charged particles

The azimuthal distribution of the charged particle multiplicity is studied for five bins in centrality and with a reaction plane orientation determined using the TCal and the most forward PCal section to avoid auto-correlations. As an example of such a double differential distribution the data for the intermediate centrality bin are shown in Figure 7 both in a three-dimensional representation and as a few slices at certain η values. A pronounced dipole component and its sign change at mid-pseudorapidity are immediately obvious. Closer inspection reveals in addition a quadrupole component, easily visible *e.g.* in Figure 7 around $\eta = 1.7$ where the dipole moment vanishes. Figure 8a shows the corrected first and second moments of the Fourier decomposition for all five centrality bins. The error bars reflect for each centrality the typical statistical errors as well as systematic errors connected to variations of the experimental conditions during the run (e.g. beam position). These were obtained by subdividing the entire data sample into subsamples (runs of 100 k events) and obtaining the standard deviation of the results from these subsamples. The two different windows used to determine the reaction plane lead, after correction for resolution, to very similar results. From this comparison we conclude that the relative systematic errors in the corrected coefficients v_1 and v_2 which are mostly determined by the correction for the reaction plane resolution are less than 10 and 20 % , respectively. For very small values of v_1 and v_2 we estimate absolute systematic errors of 0.005.

The finite dipole component v_1 represents directed sideward flow of charged particles in qualitatively the same way as seen in our previous study of E_T [7]. The dipole component shows a characteristic zero-crossing around mid-pseudorapidity and is nonzero elsewhere for all centralities chosen. The sign of the charged particle flow is such that on average charged particles go in the same direction as the transverse energy. However, the anisotropy is small,

at most 0.03. There is a subtle change in shape of the η dependence and in the location of the zero crossing with centrality.

We also find a nonzero quadrupole component which is even smaller, at most 2 % after correction. But the deviation from zero is significant as can be judged from the projection in Figure 7. There is no visible pseudorapidity dependence of v_2 . The positive values of v_2 imply enhanced yields in the reaction plane. Hence, the small quadrupole component we find is oriented perpendicular to the 'squeeze-out' observed at lower beam energies in the 1-2 A·GeV/c range [17] where preferential emission out of the reaction plane was established.

In a further analysis step, we determine the anisotropy of only those tracks that deposit more than four times the minimum ionizing energy loss in the silicon pad detector. This selects mostly low momentum particles, preferentially slow protons. The resulting anisotropy parameters are displayed in Figure 8 (right panel). Two general trends are noticeable as compared to the results for all charged particles displayed in Figure 8 (left). i) The magnitude of the anisotropy is significantly bigger, reaching values up to 10 %. ii) The location of the zero-crossing shifts forward in pseudorapidity. This is expected because of the difference between rapidity and pseudorapidity for more massive (less relativistic) particles combined with the fact that protons dominate this data sample while they account overall for roughly 1/3 of all charged particles. The larger magnitude of the anisotropy for more heavily ionizing particles could indicate that protons exhibit a stronger sideward flow effect than pions.

B. Transverse energy

A similar event shape analysis was performed on the transverse energy combining data from the two calorimeters TCal and PCal thus covering the range $-0.5 \leq \eta \leq 4.2$. We fit the experimental ϕ distribution of E_T relative to a reaction plane determined with any of the three windows W1, W3, and W4 that do not overlap in pseudorapidity with the E_T bin with the functional form

$$\frac{d^2E_T}{d\eta d(\phi - \Psi_1^{(1,3,4)})} = v_0(1 + \sum_1^2(2v'_n \cos n(\phi - \Psi_1^{(1,3,4)}))). \quad (8)$$

This is done for 15 centrality bins gating on PCal E_T ranges as indicated in Figure 4. After unfolding the coefficients v'_n for the reaction plane resolution two or three values are available for every η from the reaction plane measurements not overlapping in η . This provides a good check on the systematics. In order to correct for any asymmetries caused by interactions other than in the target we also evaluate the anisotropy coefficients from special *target-out* runs. The correction matters only for the two most peripheral centrality bins. In the first (second) bin it is found that the absolute correction to v_1 is of the order of 0.005 (0.001). As in the case of the charged particle analysis the systematic error is dominated by the accuracy of the correction for the reaction plane resolution and we assign a 10 % relative systematic error or an absolute systematic error of 0.005 to the corrected dipole coefficients.

Figure 9 shows the resulting dipole coefficients for a representative sample of centralities. Statistical errors were obtained in the same way as in the charged particle multiplicity analysis. The data were divided into 12 subsamples and the scatter of results from these subsamples defines the error of the mean. As a function of pseudorapidity the data in the 24 experimental bins form a quasi-continuous distribution with a smooth evolution from negative to positive values for more forward η with a zero crossing around $\eta = 1.9$. The data shown in Figure 9 can be compared to the values for three large η windows ($-0.5 \leq \eta \leq 0.8$, $0.83 \leq \eta \leq 1.85$, and $1.85 \leq \eta \leq 4.7$) used in our first analysis [7]. With the much finer segmentation in η it is now possible to verify that the vanishing of v_1 in the middle η window is indeed due to the zero crossing of v_1 around mid-pseudorapidity as we had suspected.

The evolution of v_1 as a function of centrality shows several systematic features. The location of the zero-crossing at $\eta = 1.9 - 2.0$ does not depend significantly on centrality except for the two most peripheral bins where more forward values are observed. The dependence of v_1 on pseudorapidity is characterized by an s-shaped curve with a minimum around $\eta \approx 0$ and a maximum around $\eta \approx 3.0$. Inspecting these extrema in v_1 as function of centrality, they reach maximum values in the range 130 - 270 GeV corresponding to collisions in the top

30 - 5 % centrality region. The maximum flow values backward and forward are 7 and 12 % respectively. Furthermore, the shape of the distributions in Figure 9 changes with centrality; the extrema of the s-shaped curve move closer to midrapidity for increasing centrality.

At lower beam momenta the slope of v_1 at midrapidity has been used to quantify the strength of the flow effect. For the present data the value is $dv_1/d\eta = d(\langle E_x \rangle / \langle E_T \rangle) / d\eta \approx 0.07$ around 15 % centrality where the flow effect is maximal, and it decreases to 0.04 for the highest centrality bin studied here. The values of the slope are significantly smaller than reported at lower energies [18] for a similar quantity, $d(\langle p_x \rangle / \langle p_t \rangle) / dy$, evaluated for protons. At beam kinetic energies per nucleon of 150, 250 and 400 MeV values of $d(\langle p_x \rangle / \langle p_t \rangle) / dy = 1.43, 1.23$ and 1.22 have been obtained. The increase in $\langle p_t \rangle$ or $\langle E_T \rangle$ and the increase in y make it plausible that the relative strength of the flow is smaller at AGS energies. Below we discuss a procedure to separate the flow effect of pions and nucleons and to relate η and y to obtain a more quantitative understanding of the systematics of the observed strong energy dependence. The comparison to lower energy data is resumed there.

Figure 9 together with the $dE_T/d\eta$ distribution [1] shows where the most sensitive η intervals are to determine the orientation of the reaction plane: $\eta \lesssim 0.8$ and $\eta \gtrsim 3.0$. This is in line with the results shown in Figure 5 for the experimental reaction plane resolution.

Figure 10 presents the results for the quadrupole component of the E_T distribution. For intermediate centralities (130-270 GeV, corresponding to the top 5-30 % of the geometric cross section) small but significant values of 1-2 % are observed. For more central and more peripheral collisions they decrease to zero. The statistical errors are shown in the figure, the relative and absolute systematic errors are estimated to be 20 % and 0.5 %. Quantitatively the values are very similar to the quadrupole anisotropy observed in the charged particle distributions. Again there is no significant dependence on pseudorapidity and again the values are positive, i.e. emission is enhanced in the reaction plane, not perpendicular to it.

V. COMPARISON WITH MODELS

Both global distributions in E_T and N_c and spectra of identified protons and pions have been compared [1,2,19–21] to predictions from two event generators based on hadronic cascades, RQMD [3] and ARC [4,5]. Although some discrepancies are noted, in particular a peaking in $dE_T/d\eta$ too much forward as compared to the data and proton spectra significantly steeper than the data close to midrapidity (for ARC only a spectrum half a unit away from midrapidity has been published [5]), the overall agreement otherwise is good. The slope of the proton spectra can be linked to transverse expansion of the system [22]. Analysis of the RQMD freeze-out condition indicates [23,24] that, in the cascading of many successive hadronic collisions, a collective transverse expansion is built up, but apparently for Au + Au collisions at AGS energies the model in its cascade mode underpredicts the transverse expansion velocity. With the present data we can subject the models to a different test of the collective velocities at freeze-out. By evaluating the sideward flow in the same manner as in the present analysis and comparing to the data we test the anisotropic component of the expansion, i.e. the component that carries the memory of the impact parameter and therefore may be sensitive to the equation of state of the system.

Figure 11 shows the dipole component of the azimuthal distribution of transverse energy and charged particle multiplicity for collisions of intermediate centrality ($\sigma_{\text{top}}/\sigma_{\text{geo}} = 5\text{-}15\%$) both from experiment and evaluated from events simulated with RQMD. It is apparent that the experimental anisotropies of both the charged particle and of the transverse energy distributions are quantitatively quite different with values for E_T about twice the values for N_c . The extracted flow parameters v_1 for a given particle species may differ depending on whether they were extracted from azimuthal distribution of the number density or the transverse energy density. It will be shown in the next section that this difference is not the dominant part of the effect seen. Since pions and nucleons contribute with different relative weights to E_T (composed mainly of energy deposits of p,n, π^+ , π^- , π^0) and to N_c (counting essentially the number of p, π^+ , π^-) one suspects that the observed difference in anisotropy

is due to a different behavior of pions and nucleons. Another indication for a difference between pions and nucleons is the different dipole anisotropy seen for all charged particles and heavily ionizing particles (see discussion above and Fig. 8).

RQMD reproduces neither the experimental anisotropy for E_T nor for N_c but, in agreement with the data, there is a difference between the two with, in general, more positive values of v_1 for the E_T distribution. In the model we can separate the contribution from pions and nucleons and Figure 12 shows, for the same centrality range as in Figure 11, the dipole anisotropy for protons, pions and, for comparison, also the anisotropy of E_T and N_c . Protons and pions show opposite flow effects of the same order of magnitude leading to differences and even to a change in sign between the dipole anisotropy of E_T and N_c in the range $\eta = 2 - 3$. Qualitatively this is in agreement with the feature exhibited by the data but quantitatively the model does not reproduce the data. The failure of RQMD to account for the anisotropy in E_T was already apparent in our first analysis in three large η bins [7]. A comparison of data and model for the bin $\eta = 1.85 - 4.7$ showed [8] that the model underpredicts the experimental dipole component by a factor of two. This discrepancy combined with the possible intricate cancellations of flow effects of pions and nucleons, as shown in Fig. 12, provides another motivation to separate the experimental effect according to particle species.

We have also evaluated from the RQMD simulations the quadrupole anisotropy coefficients v_2 for semicentral collisions. They are found to be very close to our experimental observation, with typical positive values of 0.01 - 0.02, and no significant pseudorapidity dependence. Further, we find that both pions and nucleons are contributing to this anisotropy with equal sign and comparable magnitude.

As far as the ARC event generator is concerned, a more limited comparison with the present data is possible by inspecting results of calculations shown in a recent preprint [25]. In this work, a comparison is made to the results of our first analysis in three coarse pseudorapidity bins and it appears that for the forward bin the dipole component is rather well reproduced by ARC. It is interesting to note that this agreement is achieved by introducing

an energy dependent treatment of the nucleon-nucleon scattering with a gradual transition from repulsive scattering at low relative energies to an equal probability for repulsive and attractive trajectories at higher energies. Using only the latter without energy dependence the flow for protons is reduced to half its value. Another interesting feature emerges from the ARC simulations. There the protons exhibit a quadrupole anisotropy with the long axis perpendicular to the reaction plane and this anisotropy vanishes as beam rapidity is approached. Both features are at variance with the present experimental observation of the orientation (in-plane) and pseudorapidity independence of v_2 .

VI. FLOW OF NUCLEONS AND PIONS

Using the present data on flow of transverse energy and charged particles we can try to separate the contribution of nucleons and pions to the flow effect. In this analysis we assume that the observed flow in the global observables E_T and N_c is a linear superposition of the anisotropy of nucleons and pions, thereby neglecting the contribution from other particle species. We denote the respective flow parameters by $v_1^{(N_c)}$ and $v_1^{(E_T)}$ and further differentiate between coefficients $v_1^{(N_c,n)}$, $v_1^{(N_c,\pi)}$, $v_1^{(E_T,n)}$, and $v_1^{(E_T,\pi)}$ for nucleons and pions, respectively. The dipole anisotropy of the two global observables can then be written as:

$$v_1^{(N_c)} = \frac{dN_c^\pi/d\eta \cdot v_1^{(N_c,\pi)} + dN_c^n/d\eta \cdot v_1^{(N_c,n)}}{dN_c^\pi/d\eta + dN_c^n/d\eta}, \quad (9)$$

$$v_1^{(E_T)} = \frac{dE_T^\pi/d\eta \cdot v_1^{(E_T,\pi)} + dE_T^n/d\eta \cdot v_1^{(E_T,n)}}{dE_T^\pi/d\eta + dE_T^n/d\eta}. \quad (10)$$

These equations can be solved for the flow parameters of pions and nucleons if one knows in addition to the measured $v_1^{(N_c)}$ and $v_1^{(E_T)}$ values: (i) the relative contribution of pions and nucleons to the charged particle and transverse energy pseudorapidity distributions, and (ii) the ratio of the flow parameters for a given particle species arising from particle or E_T azimuthal distributions, i.e. $v_1^{(N_c)}/v_1^{(E_T)}$ for pions and nucleons separately.

Proton and pion spectra have been measured for the top 7 % of centrality over nearly 4π if one employs symmetry with respect to midrapidity and combines data from E866 [20,26] and

E877 [21]. We have parameterized the measured rapidity distributions of protons and pions as Gaussian distributions and the transverse mass distributions as Boltzmann distributions with slope constants that again have a Gaussian distribution as a function of rapidity. This provides the double differential cross section $d^2\sigma/dydm_t$ for protons and pions for the full phase space. From this information distributions of transverse energy or charged particle multiplicity can be computed for any pseudorapidity. In order to test the quality of the parameterization and also the internal consistency of the data we have compared the distributions $dE_T/d\eta$ and $dN_c/d\eta$ from the parameterization to the quantities measured by E877 [1,2] with an entirely different detector system for the same centrality and excellent agreement is found for both quantities. As an alternative check we have used the relative contribution of nucleons and pions to E_T and N_c from RQMD and the absolute difference in the resulting values of v_1 for nucleons and pions is less than 0.005.

To estimate the difference in the anisotropy coefficient measured for E_T and N_c we again have used two approaches. We assume that the anisotropy (flow) is due to a displacement of the triple differential cross section $d^3\sigma/dp_x dp_y dy$ by some rapidity dependent amount $p_{x0}(y)$. This is close to our present experimental observation [8]. For moderate displacements ($p_{x0} \leq 0.15$ GeV/c; well justified in the rapidity range and for the system considered here) and a Gaussian distribution in p_x, p_y one can show that the ratio between $v_1^{E_T}$ and $v_1^{N_c}$ is $4/\pi$. To check the influence of this assumption on the resulting pion and nucleon flow, we have used events from RQMD to numerically evaluate this quantity. The resulting values v_1 for nucleons and pions are smaller by typically 0.01 (absolute difference).

With the two ingredients i) and ii) such determined and the measured flow parameters (left hand side of equations (9) and (10)) we can solve equations (9) and (10) for every pseudorapidity to extract $v_1^{E_T, n}$ and $v_1^{E_T, \pi}$. The resulting flow parameters for nucleons and pions are shown in Figure 13. One can see that indeed the difference in the flow parameters of transverse energy and charged particle multiplicity can be attributed to a distinctly different behavior of nucleons and pions. Nucleons show a pronounced flow effect, pions show a much weaker effect and a tendency to preferentially be emitted to the side opposite of the protons.

The assumptions made in this analysis lead to a correlated systematic error in the resulting flow coefficients for nucleons and pions and we estimate relative errors of 10 and 50 %, respectively. The uncertainty for pions becomes relatively large because the anisotropy found is so small.

A comparison of the data for nucleons and pions to the corresponding quantities from RQMD is also given in Fig. 13. This allows to understand the discrepancy between data and model for the global observables. The proton flow is underpredicted by the model at forward pseudorapidities and at the same time a stronger trend for pions to go the opposite way is predicted. This latter feature has been dubbed “antiflow” in the literature, a somewhat misleading term since the effect (in the code) is due to shadowing. The combination of these two effects (underprediction of nucleon and overprediction of opposite pion flow) leads to a transverse energy flow close to zero in the model for pseudorapidities less than 3 while the data show a pronounced flow effect there. At backward pseudorapidities in the model proton flow and pion shadowing nearly cancel. In the experimental data the pion shadowing is weaker than in the model and a pronounced flow in E_T is the result.

A first study of the effect of nucleon mean fields on the RQMD results for proton spectra and flow observables was presented in [24]. Although the mean field is introduced in a simplified Skyrme-type parameterization of the interaction, it is obvious that the model calculations are moving in the right direction. Introducing this additional repulsion the proton spectra become flatter, the proton flow increases and the pion shadowing is reduced (see Figures in [24]). This observation is related to the study of the energy dependent trajectories in nn scattering in the ARC simulations where leaving out the dominantly repulsive character also drastically reduces the flow prediction.

Using the extracted flow parameters for nucleons and employing once more our knowledge of the proton spectra (see above) we can evaluate $\langle p_x \rangle$ as a function of the rapidity and determine the slope $d\langle p_x \rangle/dy$ in order to compare to data available from lower beam energies. In the literature, typically a slope with respect to rapidity normalized to beam rapidity is quoted. From the present analysis we find for this slope a value of $d\langle p_x \rangle/dy/y_b = 0.10$

GeV/c. Recently, a systematics of this variable was shown for beam kinetic energies of 0.1 - 2.0 GeV [27]. In order to compare different collision systems the slope constants were divided by the sum of the cube root of target and projectile mass number. It was observed [27] that this normalized slope rises with beam kinetic energy and reaches an approximate plateau in the energy range of about 0.7 - 2.0 GeV/nucleon with values of 35 - 40 MeV/c. After normalization to the mass number of the colliding system our present analysis gives a value for this slope of 35 MeV/c, i.e. practically the same value as observed at much lower beam energies. This result is unexpected since the beam momentum and also the proton transverse momenta are much larger in our case. It is not clear why the slope of the absolute directed transverse momentum with respect to normalized rapidity should scale with beam energy.

VII. CONCLUSIONS

In summary, the azimuthal distributions of transverse energy and charged particle multiplicity were studied systematically as a function of pseudorapidity and of centrality for 10.8 A GeV/c Au + Au collisions. A pronounced dipole component or flow is observed. It crosses zero and changes sign around mid rapidity. The magnitude of this flow effect peaks at intermediate centralities and vanishes for very central collisions. In addition a much smaller quadrupole component or elliptic eventshape is observed. The long axis is oriented in the reaction plane and there is no significant rapidity dependence.

The same type of analysis has been performed on events from the generator RQMD and a flow signal is observed there as well. But it is significantly smaller in the model than in the data. A different generator, ARC, gives the correct strength of flow when the NN repulsion is softened at high collision energies.

The magnitude of the flow signal is larger in transverse energy than in charged particle multiplicity and this difference has been used to extract the flow signal of nucleons and pions separately for an intermediate centrality bin. It is found that nucleons show a pronounced

flow signal while for pions the signal is very weak and in direction opposite to the nucleon signal. The discrepancy between the data and the model can be traced to RQMD predicting a weaker proton flow and a stronger opposite pion flow as compared to the data. It has been shown in the literature that introducing a nucleon mean field will improve both aspects.

Compared to lower beam energies, in the range below 2 GeV kinetic energy per nucleon, the slope of the directed transverse momentum of protons with respect to normalized rapidity appears to be about constant while the absolute rapidity gap between target and projectile and the mean transverse momentum of protons grow significantly.

VIII. ACKNOWLEDGEMENTS

We thank the AGS staff, W. McGahern and Dr. H. Brown for excellent support and acknowledge the untiring efforts of R. Hutter in all technical matters. Financial support from the US DoE, the NSF, the Canadian NSERC, and CNPq Brazil is gratefully acknowledged. One of us (JPW) thanks the A. v. Humboldt Foundation for support, while another (WCC) was supported by the Gottlieb Daimler- and Karl Benz-Stiftung for preparation of this manuscript.

REFERENCES

- [1] J. Barrette *et al.*, E877 Collaboration, Phys. Rev. Lett. **70**, 2996(1993).
- [2] J. Barrette *et al.*, E877 Collaboration, Phys. Rev. **C51**, 3309(1995).
- [3] H. Sorge, A. von Keitz, R. Mattiello, H. Stöcker, W. Greiner, Phys. Lett. **B243**, 7(1990).
- [4] Y. Pang, T.J. Schlagel, and S.K. Kahana, Phys. Rev. Lett. **68**, 2743(1992);
- [5] S.H. Kahana, Proc. Workshop “Heavy Ion Physics at the AGS ’93”, G.S.F. Stephans, S.G. Steadman, W.L. Kehoe, eds., print MITLNS-2158, p. 263.
- [6] P. Braun-Munzinger, J. Stachel, J.P. Wessels, and N. Xu, Phys. Lett. **B344**, 43(1994).
- [7] J. Barrette *et al.*, E877 Collaboration, Phys. Rev. Lett. **73**, 2532(1994).
- [8] Y. Zhang and J.P. Wessels for the E877 Collaboration, Nucl. Phys. **A590**, 557c(1995).
T.K. Hemmick for the E877 Collaboration, Nucl. Phys. **A610** (1996) in print; W.C. Chang for the E877 Collaboration, Proc. Workshop “Heavy Ion Physics at the AGS ’96”, Wayne State Univ., August 1996, in print.
- [9] H. Sorge, H. Stöcker, and W. Greiner, Ann. Phys. **192**, 266(1989).
- [10] J. Barrette *et al.*, E814 Collaboration, Phys. Rev. Lett. **64**, 1219(1990).
- [11] J. Barrette *et al.*, E814 Collaboration, Phys. Rev. **C45**, 819(1994).
- [12] J. Simon-Gillo *et al.*, Nucl. Instrum. Methods **A309**, 427(1991); D. Fox *et al.*, Nucl. Instrum. Methods **A317**, 474(1992).
- [13] S. Voloshin and Y. Zhang, Z. Physik **C70**, 665(1996).
- [14] J.P. Alard *et al.*, FOPI Collaboration, Phys. Rev. Lett. **69**, 889(1992).
- [15] R. Brun *et al.*, Geant 3.15 User’s Guide, CERN Data Handling Divison Report No. DD/EE/84-1, revised 92-1 (unpublished).

- [16] S. Dagan and Y. Oren, Helios Note 184, CERN, unpublished.
- [17] H. Gutbrod *et al.*, Phys. Lett. **B216**, 267(1989); D. Brill *et al.*, Phys. Rev. Lett **71**, 336(1993).
- [18] H.A. Gustafsson et al., Plastic Ball Collaboration, Mod. Phys. Lett. **A3**, 1323(1988).
- [19] M.N. Rao for the E877 Collaboration, in Physics and Astrophysics of the Quark-Gluon Plasma, B. Sinha, Y.P. Viyogi and S. Raha eds., (World Scientific, Singapore, 1994), p.457.
- [20] K. Shigaki for the E866 Collaboration, Nucl. Phys. **A590**, 519c(1995).
- [21] J. Barrette *et al.*, to be submitted; R. Lacasse for the E877 Collaboration, Proc. Quark Matter '96, Nucl. Phys. **A610** (1996) in print.
- [22] P.J. Siemens and J.O. Rasmussen, Phys. Rev. Lett. **42**, 880(1979); K.S. Lee, U. Heinz, and E. Schnedermann, Z. Phys, **C48**, 525(1990).
- [23] H. Sorge, Phys. Lett. **B373**, 16(1996).
- [24] R. Mattiello, A. Jahns, H. Sorge, H. Stöcker, and W. Greiner, Phys. Rev. Lett. **74**, 2180(1995).
- [25] D.E. Kahana, Y. Pang, and E. Shuryak, preprint nucl-th/9604008.
- [26] Y. Akiba for the 866 Collaboration, Proc. Quark Matter '96, Nucl. Phys. **A610** (1996) in print.
- [27] M.D. Partlan et al., Phys. Rev. Lett. **75**, 2100(1995); J. Chance et al., preprint nucl-ex/9607008; N. Herrmann, Proc. Quark Matter '96, Nucl. Phys. **A610** (1996) in print.

IX. FIGURE CAPTIONS

Fig. 1 Experimental setup of E877. The insert shows enlarged the beam definition and the region surrounding the target.

Fig. 2 The participant calorimeter (PCal) and its segmentation, viewed from downstream.

Fig. 3 Placement relative to the target and segmentation of the silicon pad multiplicity detectors.

Fig. 4 a) Integral of the measured transverse energy spectrum for the two calorimeters TCal (dashed) and PCal (solid). The vertical axis is the cross section integrating from a given E_T up to the top end of the spectrum normalized to the geometric cross section. b) Correlation of the measured transverse energies in the two calorimeters projecting on the PCal (open circles) and on the Tcal (solid squares) scale. The error bars indicate the width (standard deviation) of the correlation. Also indicated are the centrality bins (horizontal and vertical dashed lines) used in the analysis (see text for details).

Fig. 5 Inverse correction factor for the first moment v_1 (left) and the second moment v_2 (right) due to the finite resolution of the reaction plane angle Ψ_R measurement in four different bins of pseudo-rapidity (see equation (5)). Solid histogram: correction factors for the most forward pseudorapidity bin obtained after normalizing to the 'mixed event' distribution (see text).

Fig. 6 Pseudorapidity of the particles depositing energy in a PCal cell as compared to the value corresponding to the geometric center of each cell. The error bars indicate the range of primary pseudorapidities contributing to energy deposit in a given cell.

Fig. 7 Left: Double differential charged particle distribution for the intermediate TCal centrality bin. Right: Three pseudorapidity bins of the same distribution. The solid line is a distribution with Fourier coefficients v_0, v_1, v_2 .

Fig. 8 Left: Flow parameters v_1 and v_2 for all charged particles. Right: Flow parameters v_1 extracted only for heavily ionizing charged particles (see text).

Fig. 9 Flow parameters v_1 of the E_T azimuthal distribution after correction of contributions other than from the target for selected centrality bins (PCal E_T).

Fig. 10 Flow parameters v_2 of the E_T azimuthal distribution for selected centrality bins.

Fig. 11 Comparison of the measured flow parameters $v_1^{(N_c)}$ and $v_1^{(E_T)}$ (solid symbols) for the centrality range 5-15 %. Also shown are the equivalent parameters extracted from RQMD events.

Fig. 12 Flow parameters from RQMD events for nucleons, pions, transverse energy and charged particle multiplicity for an exclusive centrality bin ranging from 5-15 %. The fluctuations are statistical.

Fig. 13 Decomposition of the flow parameters $v_1^{(E_T)}$ of nucleons and pions (solid symbols) and comparison to the extracted parameters from RQMD (open symbols) for an exclusive centrality bin ranging from 5-15 %.

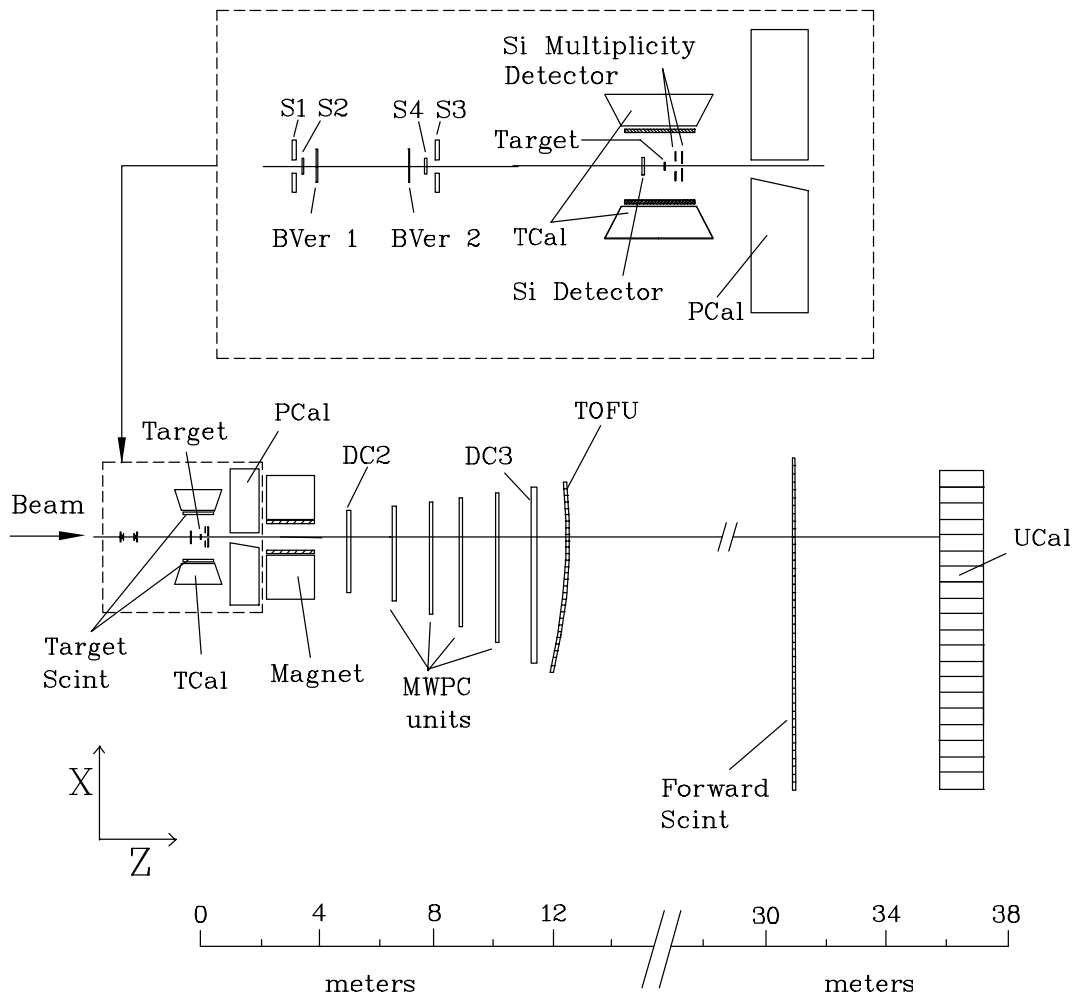


FIG. 1.

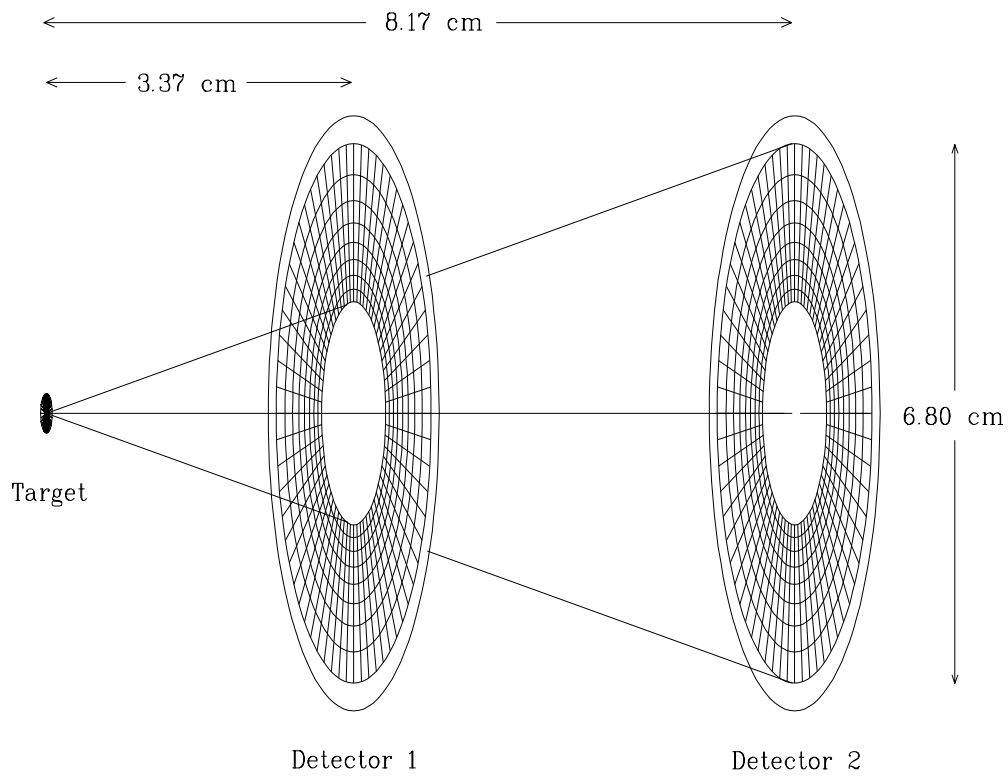


FIG. 2.

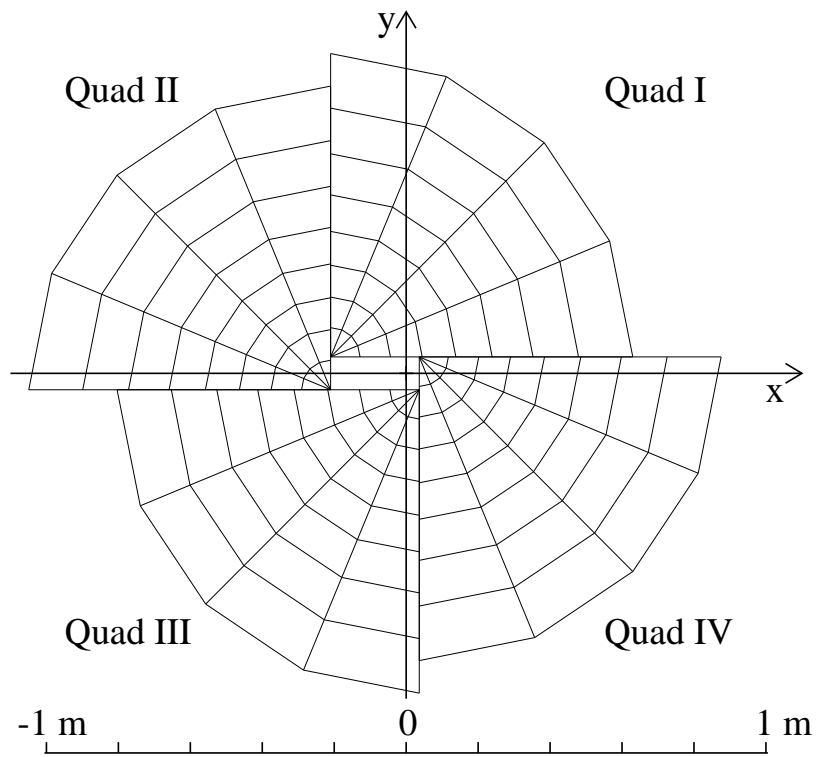
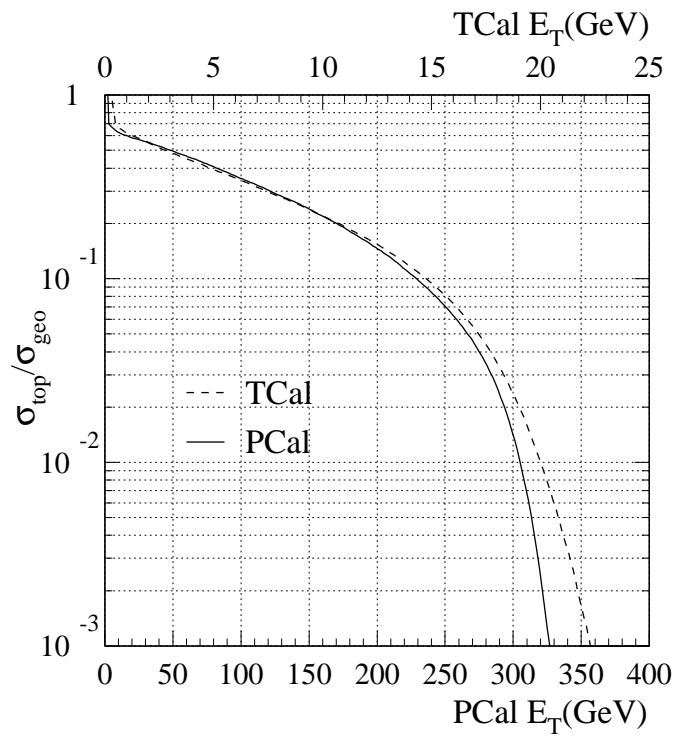
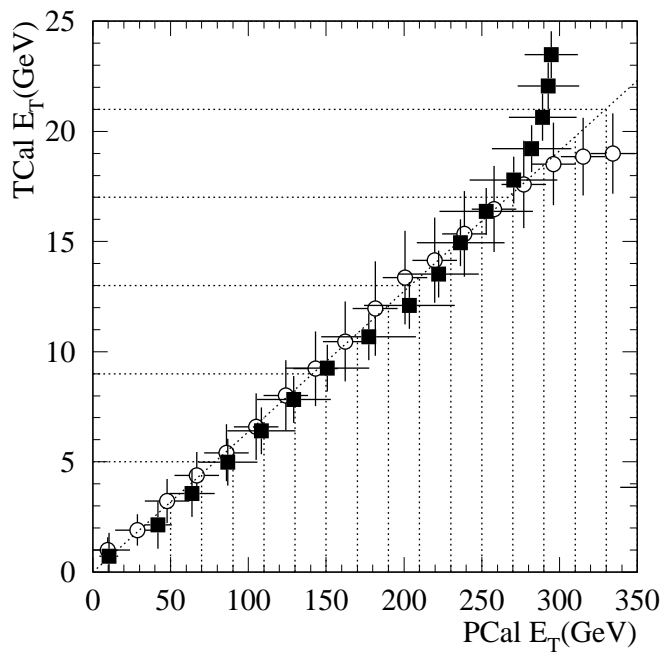


FIG. 3.



(a)



(b)

FIG. 4.

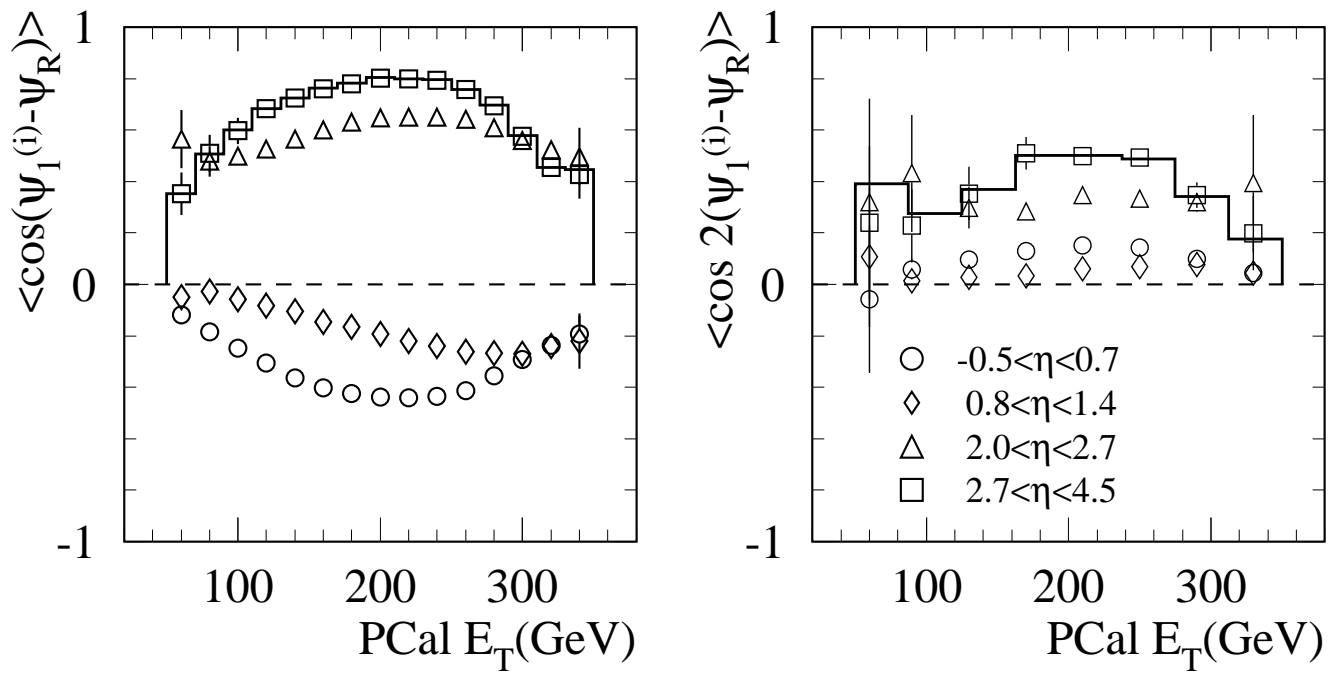


FIG. 5.

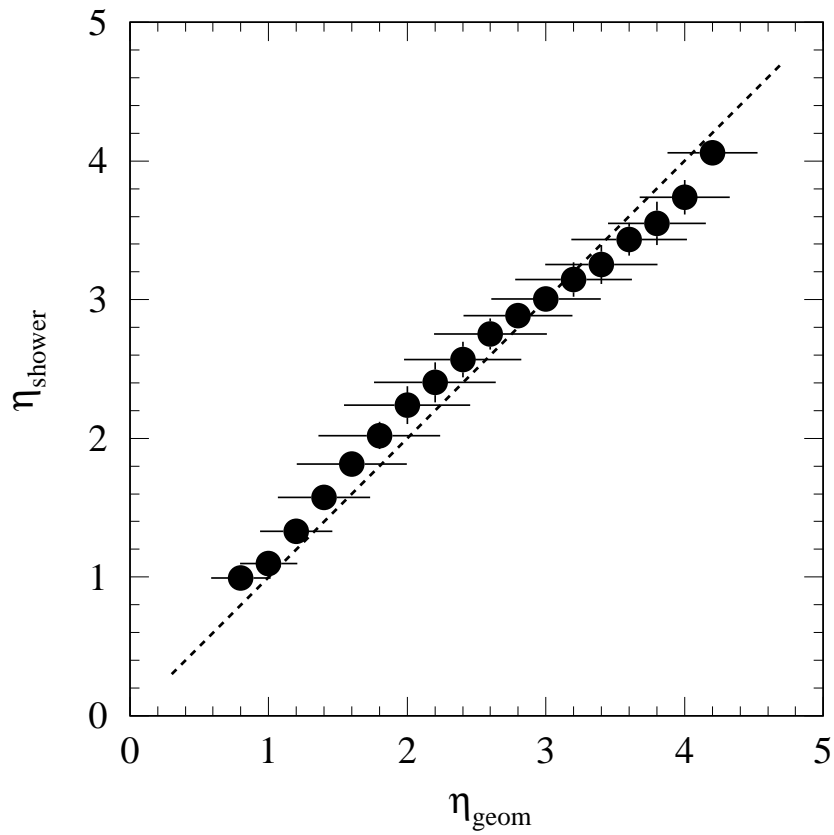


FIG. 6.

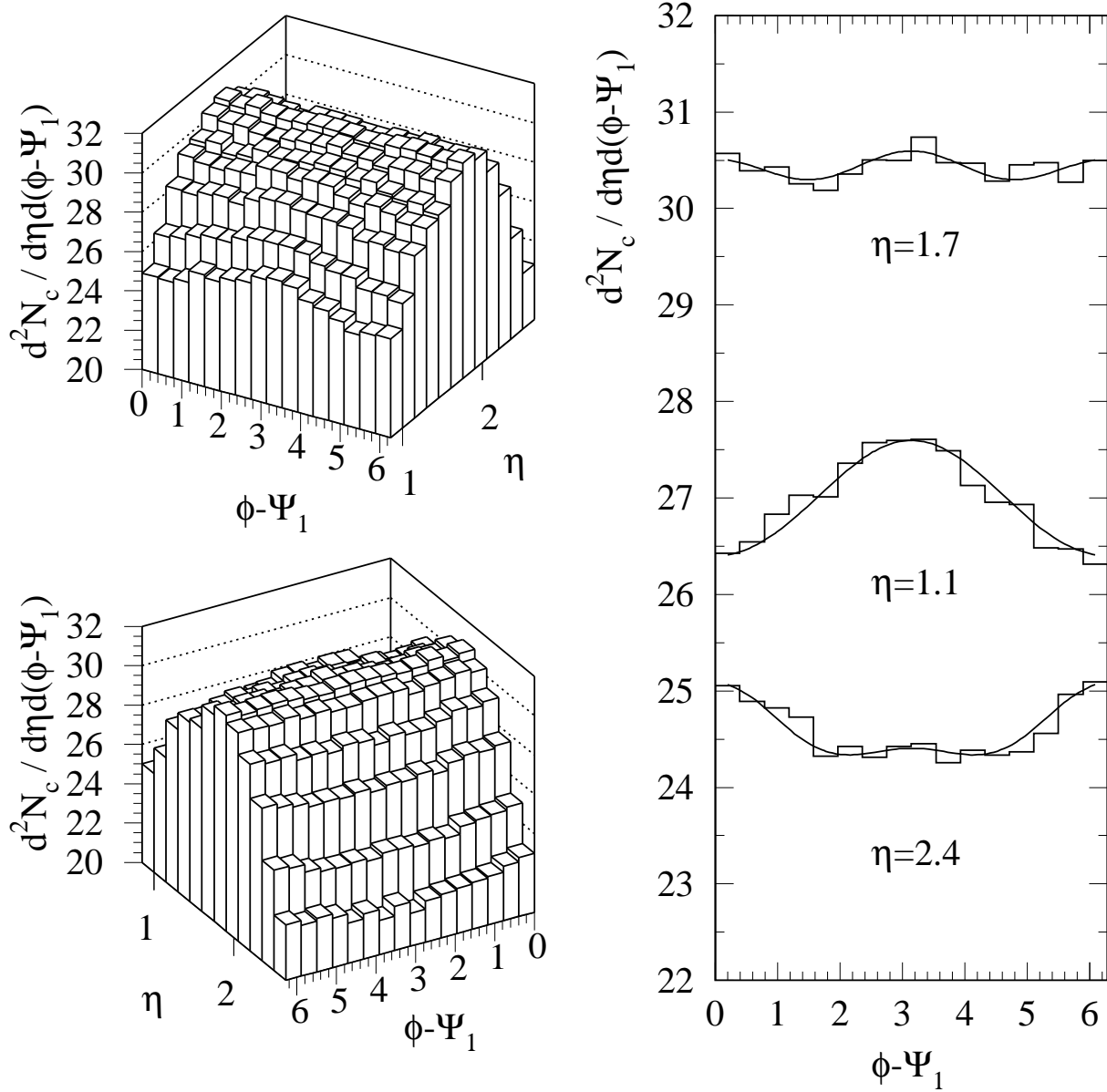


FIG. 7.

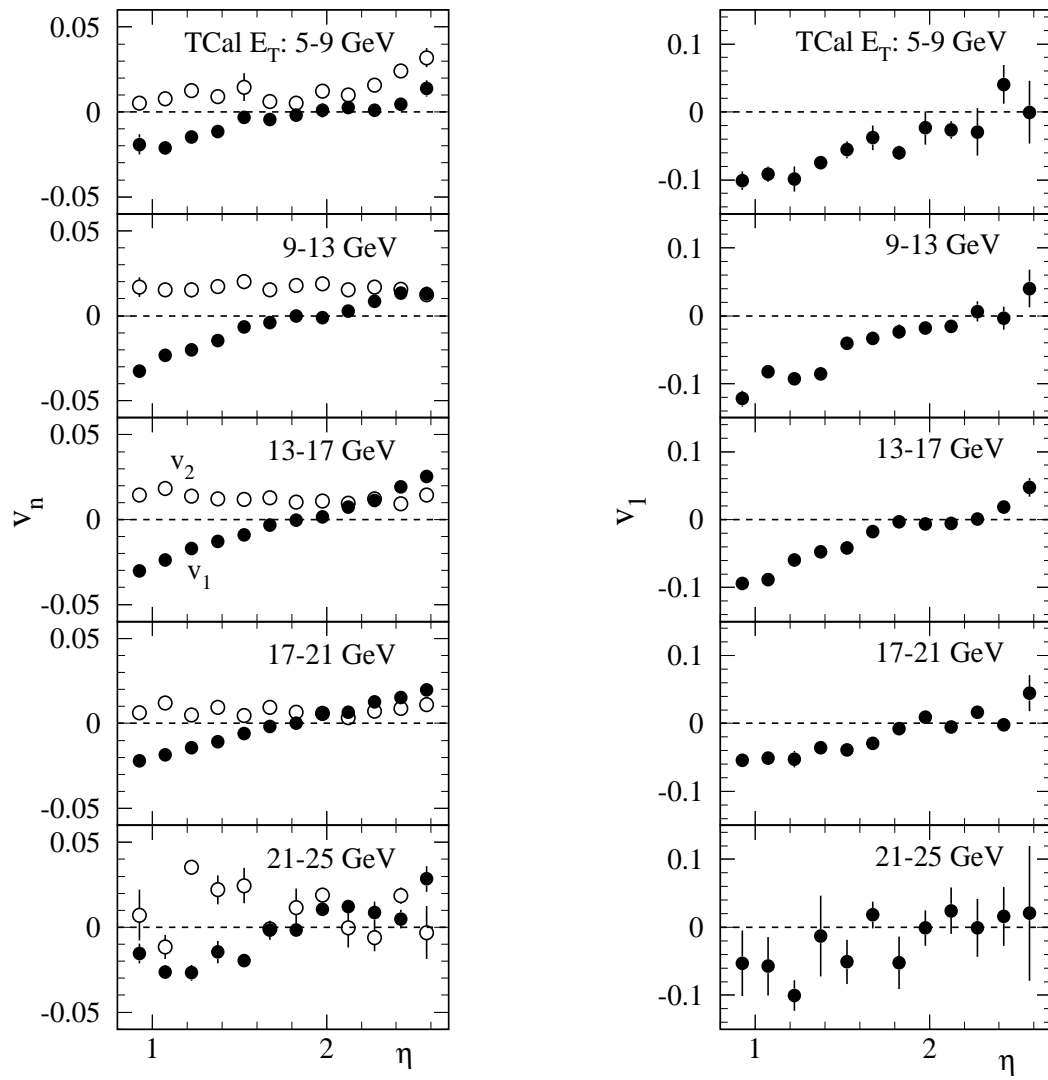


FIG. 8.

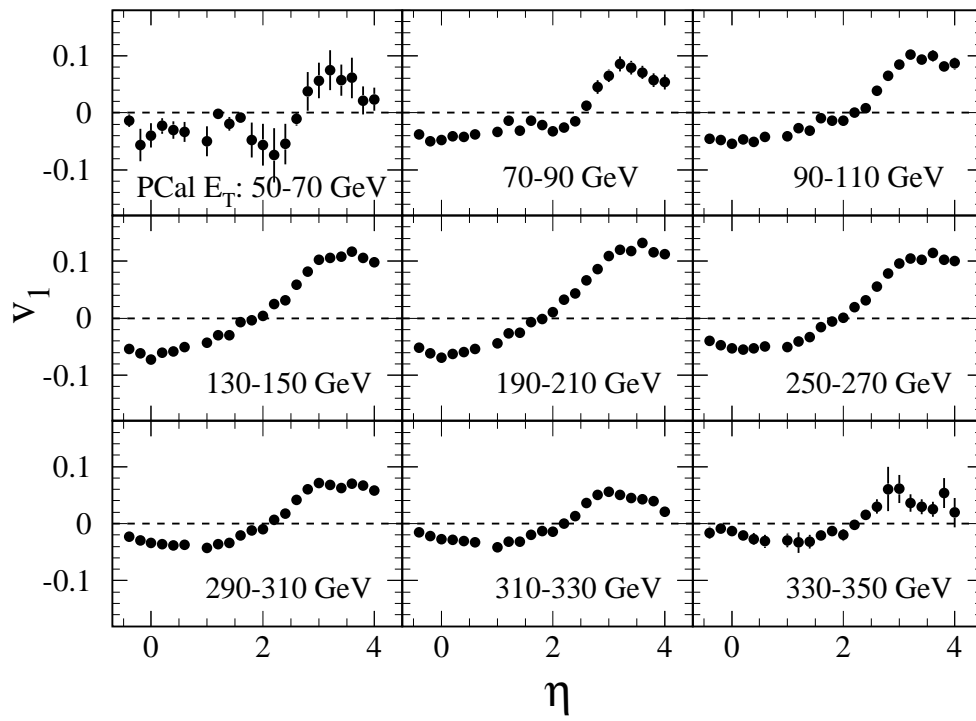


FIG. 9.

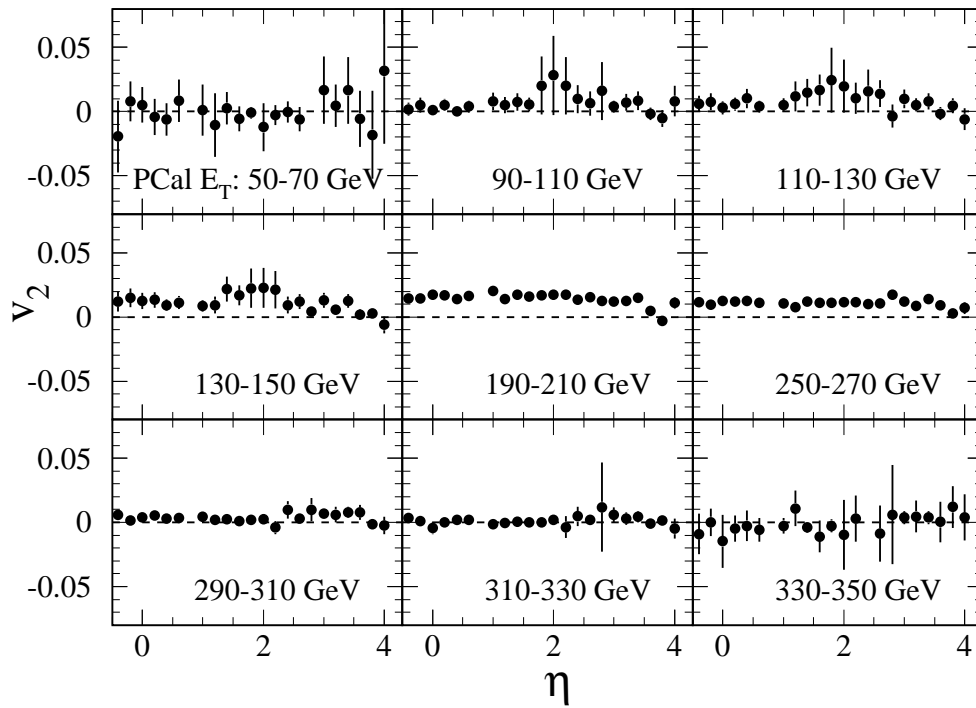


FIG. 10.

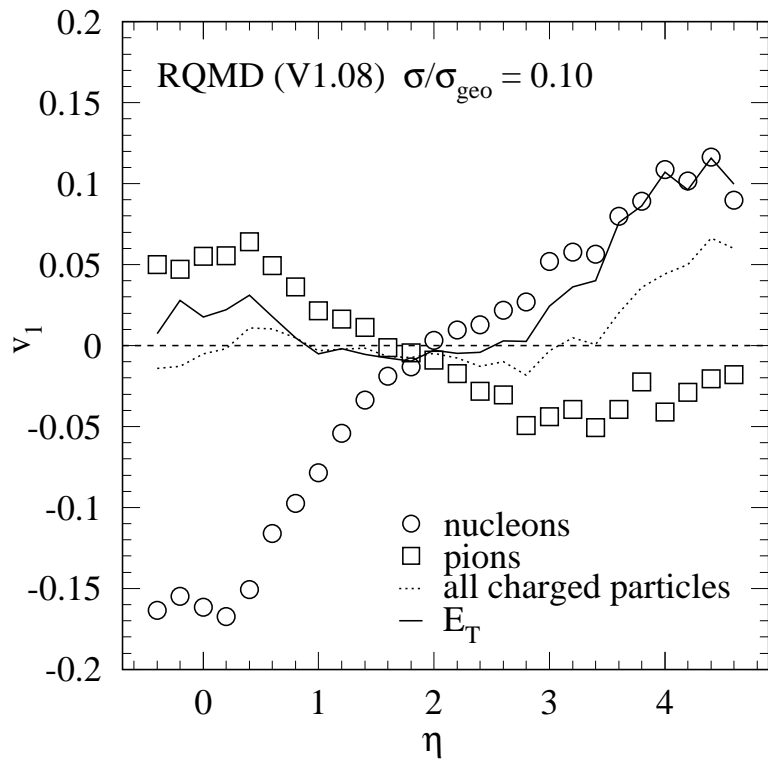


FIG. 11.

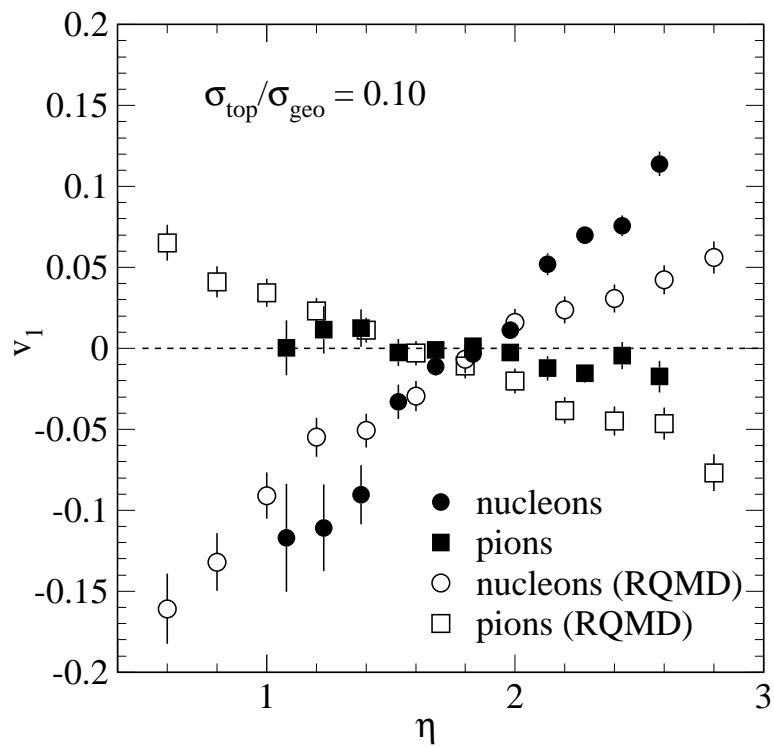


FIG. 12.

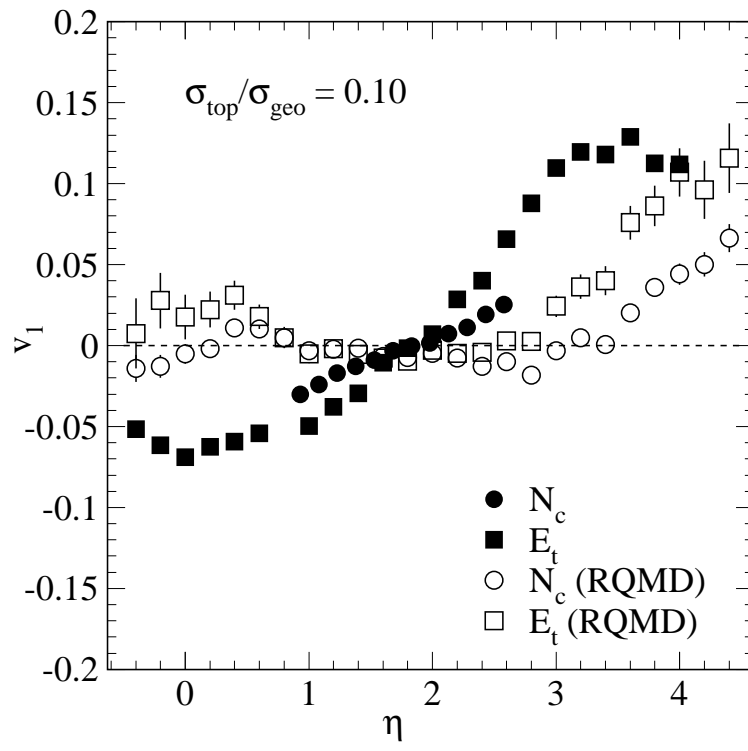


FIG. 13.